ATP8B1-mediated spatial organization of Cdc42 signaling maintains singularity during enterocyte polarization

Lucas J.M. Bruurs,[1] Lisa Donker,[1] Susan Zwakenberg,[1] Fried J. Zwartkruis,[1] Harry Begthel,[3] A.S. Knisely,[4] George Posthuma,[2] Stan F.J. van de Graaf,[5] Coen C. Paulusma,[5] and Johannes L. Bos[1]

[1]Molecular Cancer Research and Cancer Genomics Netherlands and [2]Department of Cell Biology, Center for Molecular Medicine, University Medical Center Utrecht, 3584 CG Utrecht, Netherlands
[3]Hubrecht Institute, Royal Netherlands Academy of Arts and Sciences (KNAW) and University Medical Center Utrecht, 3508 AD Utrecht, Netherlands
[4]Institute of Liver Studies, King's College Hospital, London SE5 9RS, England, UK
[5]Tytgat Institute for Liver and Intestinal Research, Academic Medical Centre, 1105 AZ Amsterdam, Netherlands

During yeast cell polarization localization of the small GTPase, cell division control protein 42 homologue (Cdc42) is clustered to ensure the formation of a single bud. Here we show that the disease-associated flippase ATPase class I type 8b member 1 (ATP8B1) enables Cdc42 clustering during enterocyte polarization. Loss of this regulation results in increased apical membrane size with scattered apical recycling endosomes and permits the formation of more than one apical domain, resembling the singularity defect observed in yeast. Mechanistically, we show that to become apically clustered, Cdc42 requires the interaction between its polybasic region and negatively charged membrane lipids provided by ATP8B1. Disturbing this interaction, either by ATP8B1 depletion or by introduction of a Cdc42 mutant defective in lipid binding, increases Cdc42 mobility and results in apical membrane enlargement. Re-establishing Cdc42 clustering, by tethering it to the apical membrane or lowering its diffusion, restores normal apical membrane size in ATP8B1-depleted cells. We therefore conclude that singularity regulation by Cdc42 is conserved between yeast and human and that this regulation is required to maintain healthy tissue architecture.

Introduction

The generation of polarized epithelial cells is paramount to proper tissue development and homeostasis. Seminal in the establishment and maintenance of stable polarity is tight spatial regulation of the small GTPase cell division control protein 42 homologue (Cdc42; Bryant and Mostov, 2008; Rodriguez-Boulan and Macara, 2014). During polarity establishment in budding yeast, Cdc42 functions as a pioneer factor because its clustered activation suffices to recruit all downstream signaling components required for bud formation (Caviston et al., 2002). To prevent ectopic bud formation, Cdc42 localization is therefore strictly governed by multiple feedback mechanisms that allow accumulation of Cdc42 at the apical membrane and ensure singularity by depleting Cdc42 elsewhere in the cell (Wedlich-Soldner et al., 2003; Slaughter et al., 2009).

By remodeling the apical plasma membrane, phospholipid flippase complexes can modulate Cdc42 signaling during yeast bud formation (Saito et al., 2007; Das et al., 2012). Nevertheless, it is unknown to what extent this mechanism contributes to polarity establishment in mammalian cells. Human phospholipid flippases of the type 4 subfamily of P-type ATPases (P_4-ATPases) have been implicated in various human disorders. Most notably, mutations in the phosphatidylserine (PS) flippase ATPase class I type 8b member 1 (ATP8B1) underlie progressive familial intrahepatic cholestasis type 1 (PFIC1), a disease hallmarked by the development of cholestasis ultimately causing liver failure. In addition, ATP8B1 mutations impose various extrahepatic symptoms including diarrhea (van der Woerd et al., 2010). These symptoms reflect the tissue distribution of ATP8B1, which is expressed only at the apical surfaces of polarized epithelial cells such as hepatocytes and enterocytes (Bull et al., 1998; van Mil et al., 2004). Although it is well established that mutations in ATP8B1 cause PFIC1, it is largely unknown which signaling pathways are affected by ATP8B1 loss and how this contributes to pathogenesis in PFIC1.

Correspondence to Johannes L. Bos: J.L.Bos@umcutrecht.nl

Abbreviations used in this paper: CMV, cytomegalovirus; CRISPR, clustered regularly interspaced short palindromic repeat; GDI, guanosine nucleotide dissociation inhibitor; HVR, hypervariable region; NEC, no endogenous Cdc42; PBR, polybasic region; PFIC, progressive familial intrahepatic cholestasis; PH, pleckstrin homology; PS, phosphatidylserine; WT, wild type.

The Rockefeller University Press $30.00
J. Cell Biol. Vol. 210 No. 7 1055–1063
www.jcb.org/cgi/doi/10.1083/jcb.201505118

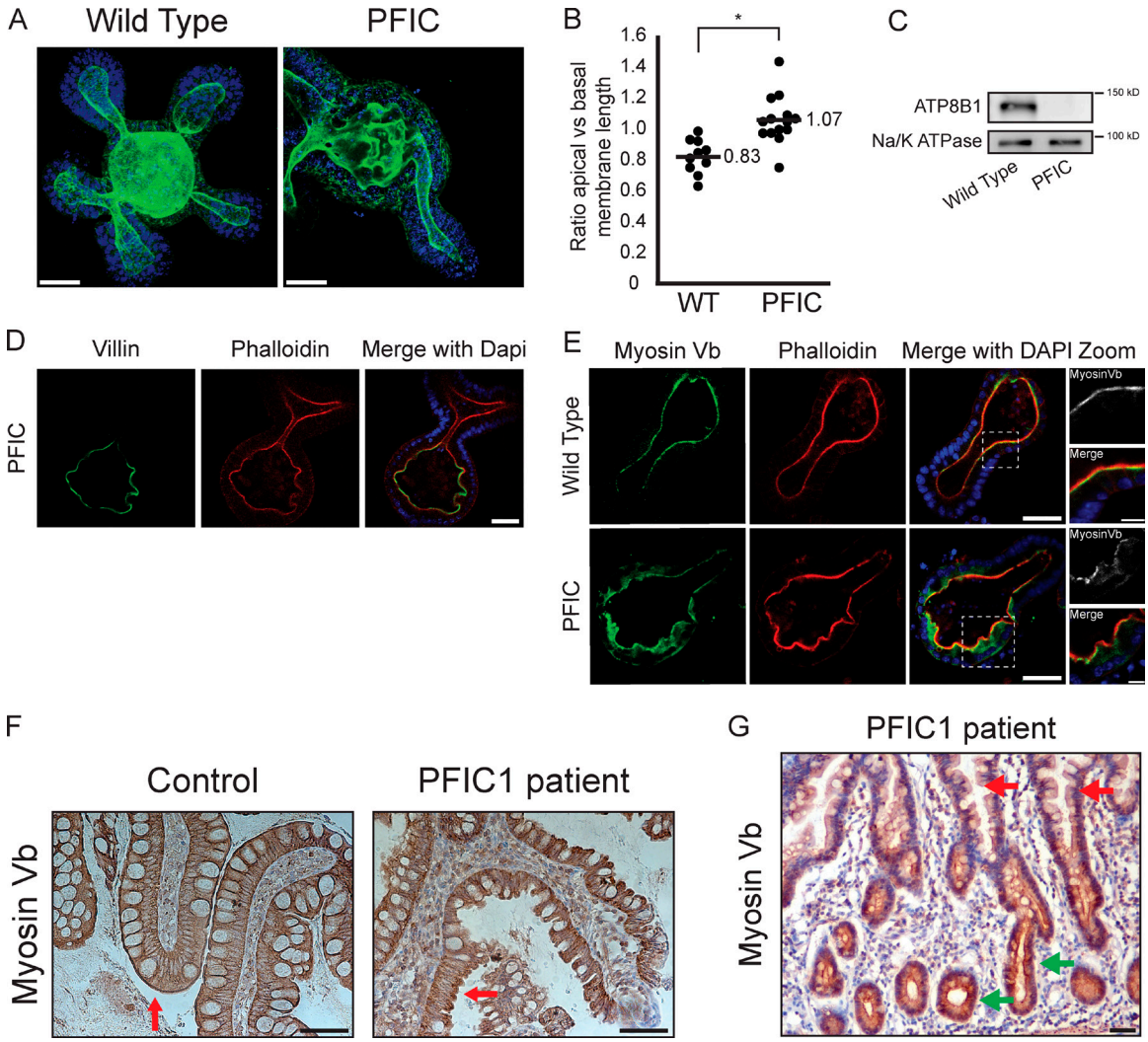

Figure 1. **Pathogenic mutations in ATP8B1 cause cell-autonomous defects in intestinal lumen formation.** (A) Maximum intensity projections of WT and PFIC small intestinal organoids fixed and stained with phalloidin (green) and DAPI (blue). (B) Ratio of apical versus basal membrane length of WT (n = 11) and PFIC organoids (n = 15). *, P < 0.0002. (C) Western blot of lysates from WT and PFIC organoids probed for ATP8B1 and Na/K ATPase. (D) PFIC organoid staining for the enterocyte marker villin, phalloidin, and DAPI. (E) WT and PFIC organoids stained for the apical endosomal marker myosin Vb. (F) Control and PFIC1 patient ileum samples stained for myosin Vb. Red arrows highlight apical myosin Vb staining. (G) Ileal sample from PFIC1 patient immunostained for myosin Vb. Red arrows highlight villi, and green arrows highlight crypts. Bars: (A, D, and E [left]) 35 µm; (E, zoom) 10 µm; (F and G) 25 µm.

Results and discussion

ATP8B1 loss affects apical membrane architecture

To investigate the mechanistic consequences of ATP8B1 loss, we generated small intestinal organoid cultures derived from an *ATP8B1*$^{G308V/G308V}$ mouse ("PFIC organoids"). The G308V mutation destabilizes the ATP8B1 protein, resulting in its functional loss (Fig. 1 C; Pawlikowska et al., 2004; Paulusma et al., 2006).

In PFIC organoids we observed structural defects in the apical membranes of the enterocytes that form the central lumen. Whereas wild-type (WT) organoids form a sphere-shaped lumen with a smooth continuous apical brush border, PFIC organoids have unstructured lumina with larger apical membranes and irregularly shaped brush borders (Fig. 1, A and B). These structural abnormalities are not observed in the crypts of PFIC organoids (Fig. 1 D), which is in agreement with the limitation in intestinal expression of ATP8B1 to differentiated enterocytes (van Mil et al., 2004).

Apical membrane generation is critically governed by recycling endosomes that deliver signaling proteins to the nascent apical membrane (Bryant et al., 2010; Dhekne et al., 2014). We found that concomitant with the defects in lumen architecture in PFIC organoids, the global distribution of apical endosomes was diffusely scattered, as determined by myosin Vb staining (Fig. 1 E). Importantly, in PFIC organoids the apical membrane marker phosphorylated Ezrin/Radixin/Moesin (pERM) and the basolateral marker CD71 segregated normally, and apical tight junctions were present, as judged by ZO-1 staining, demonstrating that overall polarity is intact in PFIC organoids (Fig. S1, A–C). To demonstrate further that ATP8B1 loss causes diffuse localization of apical endosomes, we stained biopsy specimens from healthy and PFIC1 small intestine mucosa for myosin Vb. We found that apical accumulation of myosin Vb is diminished and observed irregularities in apical membrane organization in PFIC1 patient enterocytes, similar to what was found in mouse PFIC organoids (Fig. 1 F). Furthermore, myosin Vb was normally enriched at the luminal membrane in the crypts of PFIC1

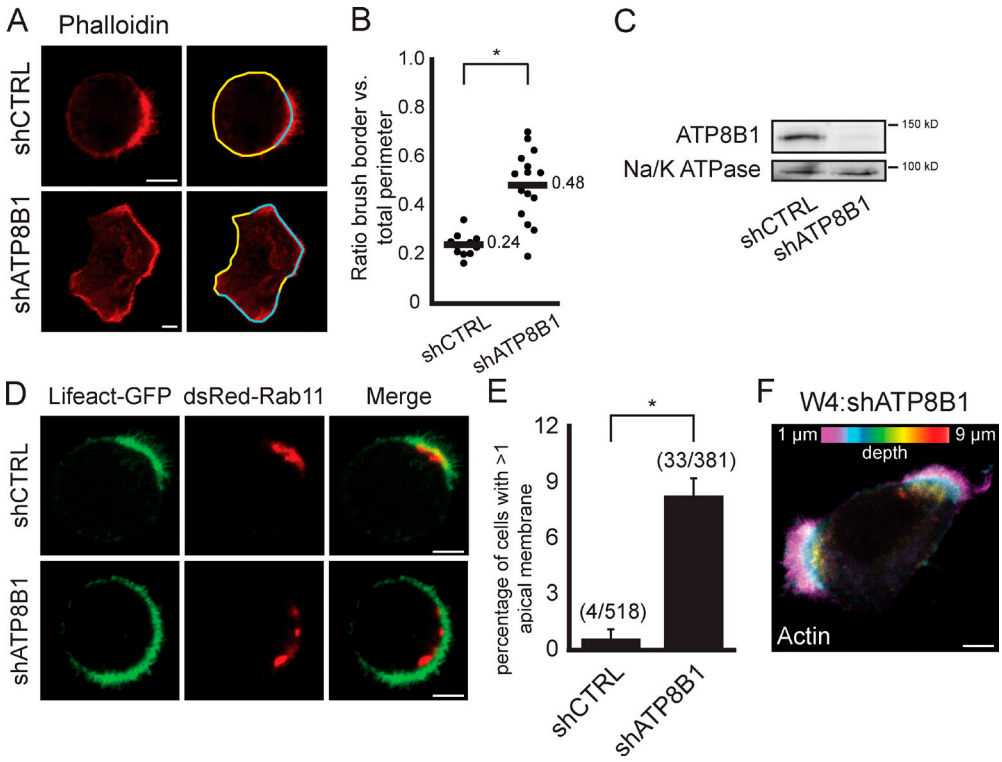

Figure 2. **Loss of ATP8B1 in polarized Ls174T:W4 cells results in the formation of an enlarged apical membrane and causes loss of singularity.** (A) Polarized Ls174T:W4 cells infected with control short hairpin or shATP8B1 stained with phalloidin to visualize the actin cytoskeleton. Blue outlining indicates apical membrane, and yellow outlining indicates basolateral membrane. (B) Apical membrane size quantified by determining the fraction of the plasma membrane bearing microvilli as visualized by actin staining. *, $P < 0.00002$. (C) Western blot of W4 cell and ATP8B1-depleted W4 cell lysates probed for ATP8B1 and Na/K ATPase. (D) Localization of the apical recycling endosomal marker dsRed-Rab11 in control- and ATP8B1-depleted W4 cells. (E) Quantification of cells with multiple brush borders in polarized control or ATP8B1-depleted W4 cells. Numbers in parentheses indicate total number of cells with multiple apical membranes in three independent experiments. Error bars are SEM from three experiments. *, $P < 0.0003$. (F) Example of ATP8B1-depleted cell that has formed two discrete brush border patches. Bars, 5 µm.

mucosa (Fig. 1 G). Evidence that ATP8B1 functions in vivo to control apical membrane size and lumen formation is additionally provided by the findings that *ATP8B1*$^{G308V/G308V}$ mice, which do not develop cholestasis (Paulusma et al., 2006), do form enlarged bile canalicular lumina (Fig. S1, D and E) and that PFIC1 patients have altered bile canalicular lumen morphology (Bull et al., 1997), additionally demonstrating that this effect is not limited to the intestine.

ATP8B1 maintains singularity in apical membrane formation

To study the molecular mechanism via which ATP8B1 deficiency affects apical membrane formation, we used the Ls174T:W4 cell line as a model system for enterocyte polarization. In W4 cells, doxycycline-induced expression of STE20-related kinase adapter protein (STRAD) drives the cytosolic activation of liver kinase b1 (LKB1), which is sufficient to polarize these cells in the absence of cell–cell contacts (Baas et al., 2004). During W4 cell polarization, an apical brush border is formed and ATP8B1 localization is restricted to the apical domain (Fig. S2 A). In W4 cells with stable knockdown of ATP8B1, doxycycline-induced polarization resulted in appearance of microvilli over a larger part of the cell than in W4 cells that expressed control shRNA (Fig. 2, A–C). These microvilli stained positive for villin, demonstrating the formation of a bona fide brush border, and other polarity markers segregated normally compared with control W4 cells (Fig. S2, B–D). As in PFIC organoids, depletion of ATP8B1 from W4 cells resulted in multiple foci of Rab11-positive recycling endosomes (Fig. 2 D). The dispersal of recycling endosomes spanned the enlarged brush border in ATP8B1-depleted cells and thus correlated with apical membrane size. Next to apical membrane enlargement and Rab11 endosome dispersal, knockdown of ATP8B1 in the W4 cells also caused the formation of multiple, discrete apical membrane patches in a fraction of cells, indicative of a singularity defect (Fig. 2, E and F). In yeast, singularity in budding is ensured by spatial confinement of the small GTPase Cdc42 into a single cluster at the incipient bud site (Caviston et al., 2002; Slaughter et al., 2009). To test whether Cdc42 is also important to ensure singularity in apical membrane generation during W4 cell polarization, we used clustered regularly interspaced short palindromic repeat (CRISPR)/Cas9–mediated gene disruption to generate W4 cells that have no endogenous Cdc42 (NEC [W4:NEC]). These Cdc42 knockout cells retained the ability to generate an apical brush border (Fig. 3 C). Nevertheless, W4:NEC cells violated singularity, as demonstrated by the appearance of multiple foci of recycling endosomes and the presence of many cells that formed multiple brush borders (Fig. 3, A and B). This singularity defect could be rescued by reintroducing WT YFP-Cdc42, excluding potential CRISPR/Cas9 off-target effects (Fig. 3 B). Therefore, we conclude that Cdc42 is required to ensure the formation of a single apical membrane during W4 cell polarization.

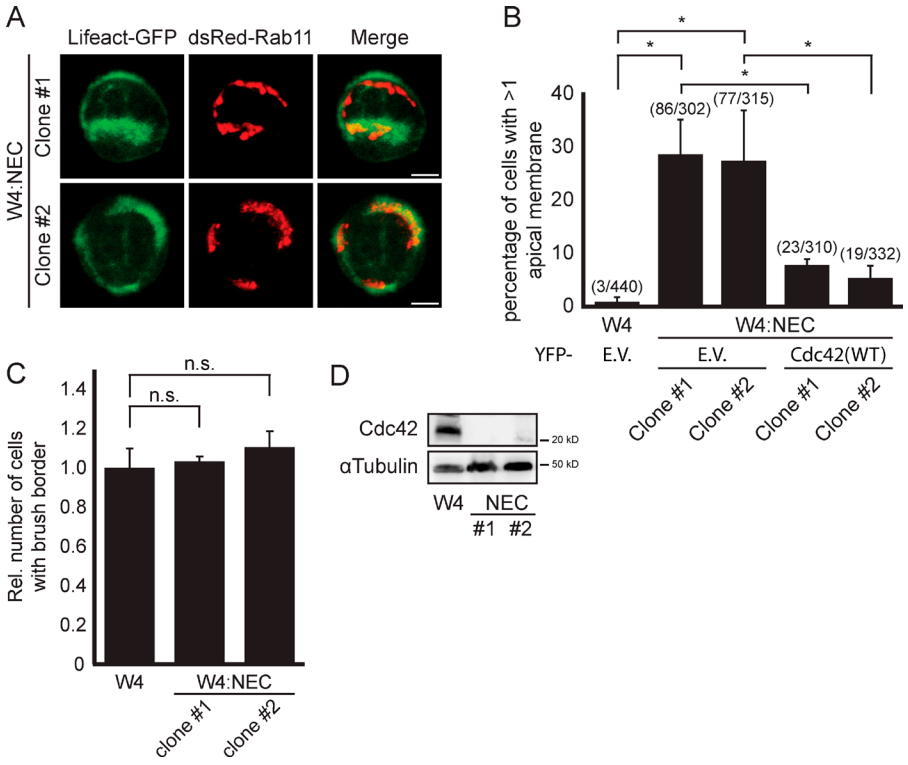

Figure 3. **Cdc42 knockout cells form multiple brush borders and have dispersed recycling endosome localization.** (A) Maximum intensity projections of polarized W4:NEC cells expressing dsRed-Rab11 and Lifeact-GFP. Bars, 5 µm. (B) Quantification of cells with multiple brush borders in polarized W4 cells or W4:NEC cells expressing YFP or YFP-Cdc42. Numbers in parentheses indicate total number of cells with multiple apical membranes in three independent experiments. Error bars are SEM from three experiments. *, $P < 0.003$. E.V., empty vector. (C) Quantification of brush border formation in W4:NEC cells. Error bars are SEM from three experiments. n.s., $P > 0.05$. (D) Western blot of W4 cell or W4:NEC cell lysates probed for Cdc42 and α-tubulin.

ATP8B1 is required for apical clustering of Cdc42

To maintain singularity during yeast budding, Cdc42 is subjected to strict spatial regulation (Howell et al., 2009; Slaughter et al., 2009). We thus questioned whether the singularity defect observed in ATP8B1-depleted W4 cells originated from altered Cdc42 localization. Indeed, whereas in W4 cells YFP-Cdc42 is enriched at the clustered apical membrane, in ATP8B1-depleted W4 cells Cdc42 localization is dispersed and is poorly enriched at the apical membrane (Fig. 4, A and B). Next, using the Cdc42(D185) mutant, we investigated whether the dispersed localization of Cdc42 in ATP8B1-depleted W4 cells caused apical membrane enlargement. By introducing a negative charge into the polybasic region (PBR) of Cdc42, the S185D mutation abrogates electrostatic interaction with negatively charged membrane lipids: whereas WT Cdc42 can interact with PS and phosphatidic acid in vitro, the Cdc42(D185) mutant has lost the ability to bind these lipids (Fig. 4 D). When expressed in polarized W4 cells, YFP-Cdc42(D185) was dispersed, like WT Cdc42 in ATP8B1-depleted W4 cells (Fig. 4 A). Importantly, expression of YFP-Cdc42(D185) in W4 cells resulted in failure of apical membrane clustering like that in ATP8B1-depleted W4 cells (Fig. 4 C). We therefore conclude that dispersed localization of Cdc42 causes apical membrane enlargement in polarized W4 cells. To demonstrate that improper clustering of Cdc42 at the apical membrane causes apical membrane enlargement in ATP8B1-depleted cells, we replaced the C-terminal hypervariable region (HVR) of Cdc42 with the pleckstrin homology (PH) domain of phospholipase Cδ (PLCδ), which binds phosphatidylinositol 4,5-bisphosphate (PI(4,5)P2). This apically enriched membrane lipid is localized independently of ATP8B1 and thus provides an alternative apical localization signal (Martin-Belmonte et al., 2007; Gervais et al., 2008). Indeed, this fusion protein completely recued the enlarged apical membrane in ATP8B1-depleted cells (Fig. 4, F and G).

ATP8B1 limits Cdc42 mobility at the apical membrane

The dispersed localization of Cdc42 in ATP8B1-depleted W4 cells suggests that ATP8B1 functions to tether Cdc42 at the apical membrane, which is required for Cdc42 to direct apical membrane clustering and maintain singularity. To measure apical membrane association of Cdc42, we fused the HVR of Cdc42, either WT or D185, with the photoconvertible Dendra fluorescent protein. Upon expression of these probes in polarized W4 cells, local green to red photoconversion in the brush border is followed by gradual loss of red signal from this region as a result of diffusion (Fig. 5 A). Therefore, the rate of signal decline from the converted region reflects the ability of these probes to be maintained at the apical plasma membrane. As full-length Cdc42(D185) induces apical membrane enlargement, we used the isolated HVRs to monitor intrinsic membrane association without disturbing cell morphology.

Means of normalized decline traces revealed that the D185 mutant was lost from the apical membrane more rapidly than the WT probe (mean half-life 132.5 s vs. 81.1 s; Fig. 5, B–D). The WT probe was evicted from the apical membrane more rapidly in ATP8B1-depleted cells than in control W4 cells, at a rate similar to the D185 mutant in control W4 cells (93.3 s and 81.1 s, respectively; Fig. 5, B–D). In contrast, the eviction rate of Dendra-Rap2A(HVR), which does not contain a PBR but requires palmitoylation for plasma membrane association, was unaffected by ATP8B1 knockdown (Fig. S3, A and B). The increased mobility of Cdc42 in ATP8B1-depleted cells critically impedes the ability of Cdc42 to maintain a clustered apical membrane because Cdc42 mutants that have stronger membrane association, resulting from introduction of additional basic residues, could restore normal apical membrane size in ATP8B1-depleted cells (Fig. 5, E and F; and Fig. S3 C).

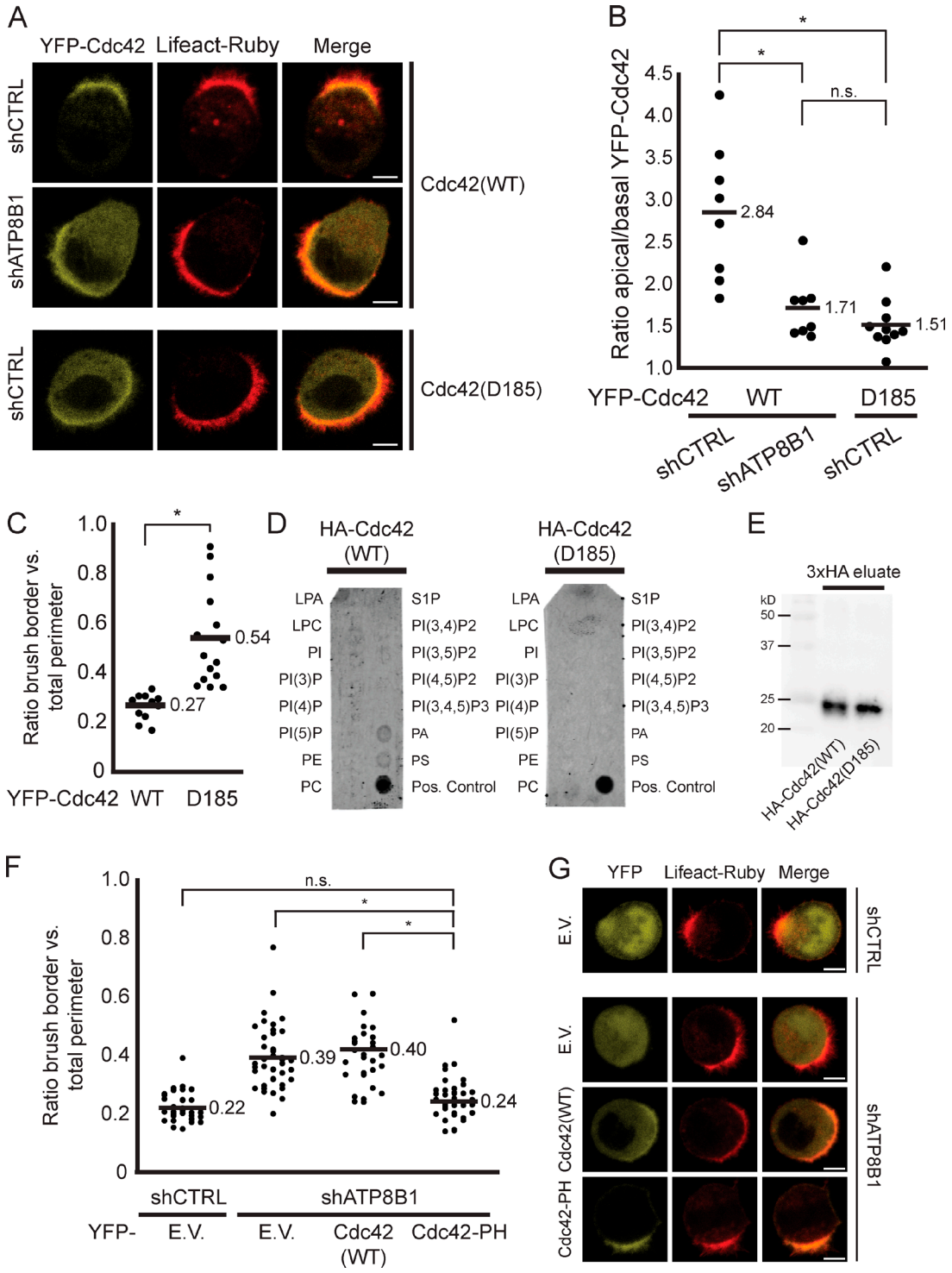

Figure 4. **Loss of clustered Cdc42 localization causes apical membrane enlargement downstream of ATP8B1.** (A) Localization of YFP-Cdc42, WT or D185, in polarized control- or ATP8B1-depleted W4 cells. (B) Quantification of apical enrichment of YFP-Cdc42 in polarized W4 cells. Quantified as the ratio of the mean signal intensity between apical and basal membrane localized YFP-Cdc42. *, $P < 0.005$; n.s., $P > 0.05$. (C) Quantification of apical membrane size in polarized W4 cells expressing YFP-Cdc42 WT or D185. *, $P < 0.0002$. (D) HA-Cdc42(WT) and HA-Cdc42(D185) binding profile to membrane-spotted phospholipids. (E) Western blot for HA tag of immunoprecipitation eluates that were added to the lipid-spotted membranes in D, demonstrating that equal amounts of HA-Cdc42 were allowed to bind. (F) Quantification of apical membrane size in control W4 cells or ATP8B1-depleted W4 cells expressing YFP, YFP-Cdc42(WT), or YFP-Cdc42-PH. *, $P < 0.00001$; n.s., $P > 0.05$. E.V., empty vector. (G) Representative images of polarized W4 cells, control or ATP8B1 depleted, expressing YFP, YFP-Cdc42(WT), or YFP-Cdc42-PH in combination with the actin marker Lifeact-Ruby. Bars, 5 µm.

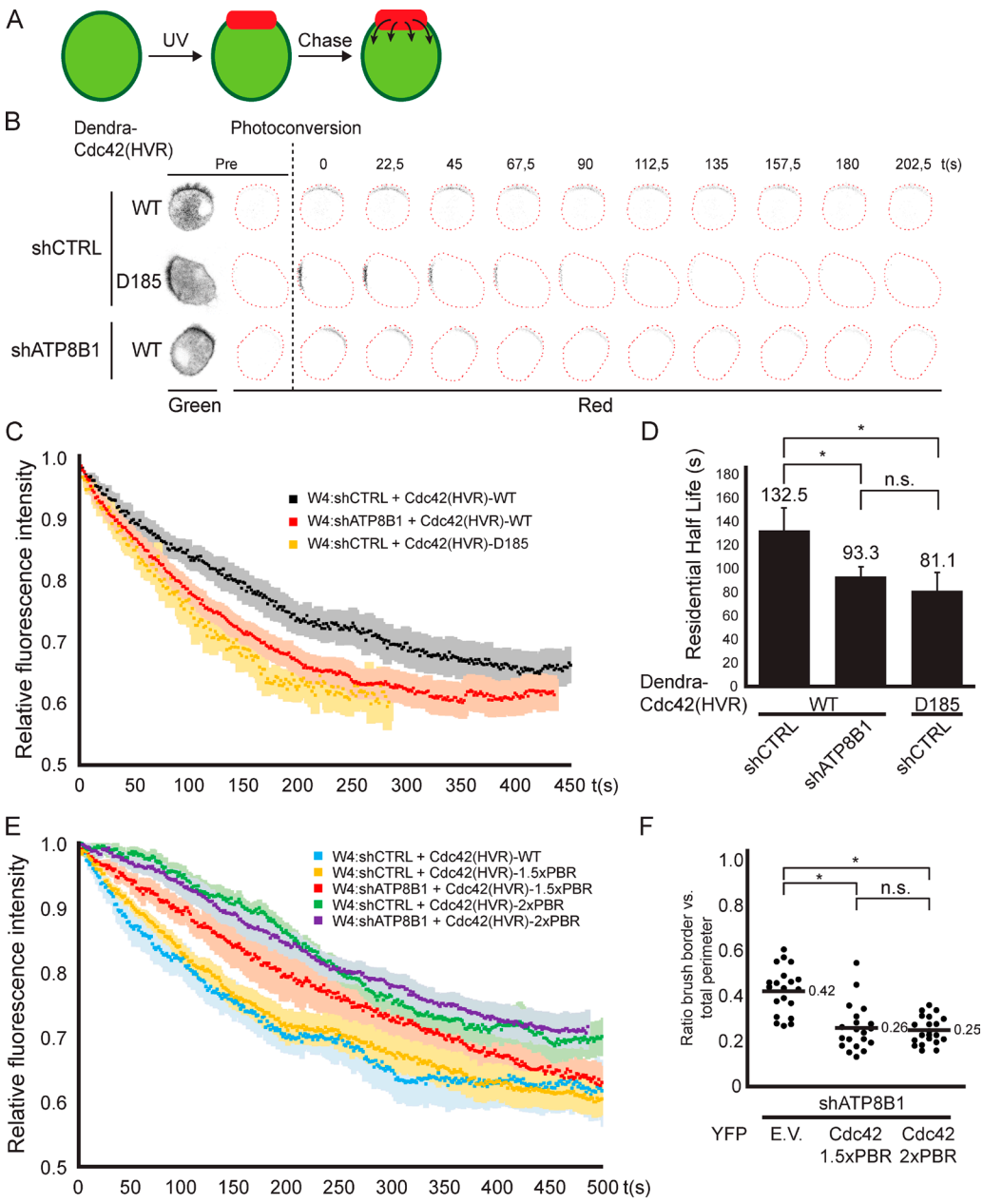

Figure 5. **Loss of ATP8B1 increases the apical diffusion rate of Cdc42.** (A) Schematic representation of the experimental setup used to determine the apical membrane diffusion rate. (B) Still images from representative photoconversion videos based on which the dissociation traces in C were generated. (C) Mean normalized dissociation traces for control W4 cells expressing Dendra-Cdc42(HVR) WT (n = 11) or Dendra-Cdc42(HVR) D185 (n = 6) or ATP8B1-depleted cells expressing Dendra-Cdc42(HVR) WT (n = 17). (D) Residential half-lives determined from mean decay traces shown in C using curve fitting. Statistics were performed using half-lives from individual cell traces. Error bars represent SEM. *, $P < 0.05$; n.s., $P > 0.05$. (E) Mean normalized dissociation traces for control or ATP8B1-depleted W4 cells expressing Dendra-Cdc42(HVR) WT (n = 6), 1.5×PBR (shCTRL n = 7, shATP8B1 n = 9), or 2×PBR (shCTRL n = 12, shATP8B1 n = 8). (C and E) Light areas indicate SEM. (F) Apical membrane size in ATP8B1-depleted W4 cells expressing YFP, YFP-Cdc42(1.5×PBR), or YFP-Cdc42(2×PBR). *, $P < 0.00002$; n.s., $P > 0.05$. E.V., empty vector.

Conclusion

We have established that loss of the mammalian flippase ATP8B1 results in defects in apical membrane architecture and abolishes singularity in recycling endosomal directionality. These defects are likely to contribute to the pathogenesis of PFIC1 in a bile acid–independent, cell-autonomous manner. Depletion of ATP8B1 causes a singularity defect, as demonstrated by the appearance of cells that have multiple apical domains but also as illustrated by the multiple clusters of Rab11 recycling endosomes in ATP8B1-depleted cells. The enlarged apical membrane in ATP8B1-depleted cells may mask potential multiplicity and likely explains why multiple brush borders are only observed in a fraction of cells.

We and others have demonstrated that Cdc42, the master regulator of singularity during yeast budding, interacts with PS (Finkielstein et al., 2006), thus linking ATP8B1 via its preferred lipid substrate to Cdc42 localization (Ujhazy et al., 2001; Paulusma et al., 2008; Cai et al., 2009). Flippase-mediated modulation of Cdc42 membrane association also occurs during yeast budding (Saito et al., 2007; Das et al., 2012). Nevertheless, in

contrast to ATP8B1, these flippases function to promote Cdc42 membrane dissociation and have not been implicated in singularity regulation. Therefore, our work demonstrates for the first time that membrane remodeling by lipid flippases is crucial for Cdc42 to enforce singularity in apical membrane generation.

We show that ATP8B1 loss results in a higher mobility of Cdc42 at the apical membrane. Various mechanisms may account for Cdc42 loss from the apical cluster, including guanosine nucleotide dissociation inhibitor (GDI)–mediated extraction and lateral diffusion. These mechanisms are likely interconnected as impaired function of the PBR both weakens membrane association and increases GDI binding (Forget et al., 2002; Das et al., 2012). By using the C-terminal fragments of Cdc42, which are not bound by GDIs, the mobility observed during photoconversion experiments is GDI independent and demonstrates that ATP8B1 affects Cdc42 membrane association independent of GDP/GTP loading or GDI binding. Nevertheless, GDI-mediated extraction may act in concert to impose the diffuse localization of full-length Cdc42 in ATP8B1-depleted cells.

The ATP8B1-mediated decrease in Cdc42 mobility at the apical membrane critically affects the ability of Cdc42 to maintain singularity. Our data thus provide experimental evidence, in a mammalian context, for mathematical models of singularity in yeast that stress the importance of apical membrane diffusion as a key determinant in the establishment of a single apical domain (Marco et al., 2007; Goryachev and Pokhilko, 2008; Howell et al., 2009; Klünder et al., 2013; Slaughter et al., 2013).

Importantly, tight and adherens junctions are normally formed in intact tissue when ATP8B1 is lost and no ectopic lumina are formed, indicating that junction formation is dominant in apicobasal membrane segregation. However, the structural defects in apical membrane organization demonstrate that pathogenic loss of ATP8B1 affects lumen formation in a multicellular context and suggest a function for the evolutionary conserved process of singularity in maintaining healthy tissue architecture.

Materials and methods

Cell culture and plasmids

Ls174T:W4 cells were cultured in RPMI1640 (Lonza) supplemented with 10% tetracycline-free FBS (Lonza) and antibiotics. To induce polarization, W4 cells were cultured in medium containing 1 µg/ml doxycycline (Sigma-Aldrich) for at least 16 h. For transient transfection, W4 cells were transfected using X-tremeGene9 (Roche) according to the manufacturer's guidelines.

N-terminally tagged YFP- or HA-tagged Cdc42 proteins were generated using Gateway recombination (Invitrogen) in pcDNA3 and pMT2 backbones, respectively, and under control of a cytomegalovirus (CMV) promotor. The Cdc42 S185D mutation was introduced by site-directed mutagenesis. For the C-terminal Cdc42 mutants (PH fusion and PBR extensions), first a unique EcoR1 site was introduced after amino acid 174. This site was subsequently used to introduce the PH domain (amino acid 21–130) PCR fragment, derived from PLCδ, or the modified PBRs, generated by annealing the corresponding oligonucleotides using In-Fusion cloning reactions (Takara Bio Inc.). For photoconversion experiments, the region encoding the Cdc42 HVR (corresponding to amino acid residues 175–191) or Rap2A HVR (amino acid residues 167–183) was N-terminally fused to Dendra in pDendra-C2 under control of a CMV promotor. Lifeact-Ruby and Lifeact-GFP in pmRFP-Ruby-N1 and pEGFP-N1 under control of a CMV promotor were provided by R. Wedlich-Soldner (University of Münster, Münster, Germany), and dsRed-Rab11 in pdsRed-N1 under control of a CMV promotor was provided by J.P. Ten Klooster (Hubrecht Institute, Utrecht, Netherlands).

Antibodies

The following antibodies were used for immunofluorescence: rabbit anti-myosin Vb (1:1,000; Novus Biologicals), mouse anti-villin (1D2C3; 1:500; Santa Cruz Biotechnology, Inc.), mouse anti-CD66 (1:500; BD), mouse anti-CD71 (H68.4; 1:1,000; Life Technologies), rabbit anti–phospho Ezrin (Thr567)/Radixin (Thr564)/Moesin (Thr558) (1:250; Cell Signaling Technology), and mouse anti–ZO-1 (1A12; 1:500; Life Technologies). The following antibodies were used for Western blots: rabbit anti-ATP8B1 (H-91; 1:1,000; Santa Cruz Biotechnology, Inc.), rabbit anti-Cdc42 (11A11; 1:5,000; Cell Signaling Technology), mouse anti–Na/K ATPase (1:5,000; EMD Millipore), mouse anti-HA (12CA5; 1:5,000; Roche), and mouse anti–α-Tubulin (DM1A; 1:10,000; EMD Millipore).

Lentiviral knockdown

Ls174T-W4 cells were infected for two successive days with lentiviral shRNA constructs (Mission library; Sigma-Aldrich). Infected cells were selected for puromycin resistance (10 µg/ml) for at least 3 d. For stable knockdown of ATP8B1, three hairpins were used (target sequence shRNA #1: 5′-CGGAAGCGAATGTCTATCATT-3′, shRNA #2: 5′-CCGATGGTCTTACATAAGGAT-3′, and shRNA #3: 5′-CCACTATCTTATTGAGCAAAT-3′).

Generation of Cdc42-deficient W4 cells using CRISPR/Cas9

W4 cells were transiently transfected with pSpCas9(BB)-2A-GFP (PX458), encoding an sgRNA (5′-GAAGCCTTTATACTTACAGT-3′) targeting the first coding exon of Cdc42. Single GFP-positive cells were sorted to individual wells of a 96-wells plate using a FACSAria II flow cytometer (BD). Genomic DNA from expanded clones was isolated using the QIAamp DNA Micro kit (QIAGEN). The targeted genomic region was amplified by PCR (forward primer: 5′-GAATAGCCAGGGA TCAGAAAC-3′, reverse primer: 5′-TTGAGACCACCACTCGTTAG-3′), cloned into pGEMT (Promega), and sequenced. Absence of Cdc42 was demonstrated by Western blotting. The two clones presented are independent clonal lines generated using the same sgRNA.

Live cell imaging

Transfected W4 cells were split and seeded onto glass-bottom dishes (WillCo Wells) in the presence of 1 µg/ml doxycycline. Before imaging, medium was removed and replaced with Hepes-buffered (pH = 7.4) Leibovitz's L-15 medium (Invitrogen). Cells were imaged at 37°C using an Axioskop2 LSM510 scanning confocal microscope (Carl Zeiss) with a 63× magnification oil objective (Plan Apochromat, NA 1.4) using Zen image acquisition software (Carl Zeiss). Apical membrane size was determined using ImageJ software (National Institutes of Health) by measuring the total perimeter of the cell and the length of the membrane bearing microvilli. Mean apical membrane sizes were compared using an independent samples *t* test in SPSS with a p-value <0.05 as a cutoff for significance. Quantification of apical enrichment of YFP-Cdc42 was performed by making a line scan through the apical and basal membrane and determining the ratio between mean apical and basal membrane pixel intensities using ImageJ. Mean enrichment ratios were compared using an independent samples *t* test in SPSS with a p-value <0.05 as a cutoff for significance.

Intestinal organoid cultures

WT and PFIC organoids were cultured as described previously (Sato et al., 2009). In brief, crypts from an *ATP8B1*$^{G308V/G308V}$ mouse were isolated in 2 mM PBS/EDTA. Crypts were pelleted and resuspended

in Matrigel (BD) and plated in 24-well plates. Organoids were cultured in advanced DMEM/F12 (Life Technologies) supplemented with B27 supplement (Life Technologies), mEGF (Life Technologies), 5% R-Spondin–conditioned medium, 10% Noggin-conditioned medium, and *N*-acetyl-cysteine. Organoids were passaged every 5 d by mechanical dissociation using a Pasteur pipette.

Immunofluorescence staining on organoids

For immunofluorescence, organoids were seeded on glass-bottom dishes (WillCo Wells) after passaging. 4 d after passaging, organoids were fixed in 4% formaldehyde for 15 min at 4°C. After gentle washing with PBS, organoids were permeabilized in PBD-2T buffer (1% BSA, 10% DMSO, and 2% Triton X-100 all in PBS) for at least 4 h at 4°C. PBD-2T buffer containing primary antibody was added to permeabilized organoids and incubated overnight at 4°C. After washing with PBD-2T buffer, Alexa Fluor 488–coupled secondary antibody diluted in PBD-2T buffer together with DAPI and phalloidin–Alexa Fluor 568 was added and incubated overnight at 4°C. After washing with PBD-2T three times for 10 min, the organoids were washed twice with PBS and were stored at 4°C in PBS. Organoids were imaged using an Axioskop2 LSM510 scanning confocal microscope (Carl Zeiss) with a 40× magnification oil objective (EC PLAN-Neofluar, NA 1.3) using Zen image acquisition software. Apical membrane size was quantified by determining the ratio of apical and basal membrane at the center of the lumen using ImageJ software. Mean apical membrane sizes were compared using an independent samples *t* test in SPSS with a p-value <0.05 as a cutoff for significance.

Lipid-overlay assay

HEK293T cells were transfected with HA-Cdc42(WT) or HA-Cdc42(D185). After 3 d, cells were lysed in IPP buffer (50 mM Tris, pH 7.5, 5 mM EDTA, 0.1% Tween-20, and 350 mM NaCl) and cleared by centrifugation at 4°C. Protein A beads were precoupled with anti-HA antibody and used to precipitate HA-Cdc42 from lysates for 3 h at 4°C. After washing, HA-Cdc42 was eluted from the beads using HA peptide (Sigma-Aldrich; 0.5 mg/ml in BC300 buffer: 20 mM Tris, pH 7.9, 20% glycerol, and 300 mM KCl) by shaking for 1 h at room temperature. 10% of both eluates was loaded onto a gel for SDS-PAGE to evaluate protein recovery. PIP-Strips (Echelon Biosciences) were blocked in PIP-Strip buffer (20 mM Tris, pH 7.5, 150 mM NaCl, 3% BSA, and 0.1% Tween-20) for 1 h at room temperature. HA-Cdc42 eluates were added to the PIP-Strips and incubated for 16 h at 4°C. After washing, PIP-Strips were probed with anti-HA antibody and Alexa Fluor 690–coupled secondary antibody before detection with an Odyssey imaging system (LI-COR Biosciences).

Apical membrane eviction rates

To determine apical membrane eviction rates, W4 cells were transfected with Dendra-Cdc42(HVR), polarized, and imaged at 37°C in Hepes-buffered (pH = 7.4) Leibovitz's L-15 medium (Invitrogen). Photoconversion and imaging were performed using an SP8x microscope (Leica) equipped with a temperature- and CO_2-controlled chamber using a 63× objective (HC Plan Apochromat 63×/1.40 oil) with LAS AF image acquisition software (Leica). Photoconversion of the Dendra fluorophore was performed with a pulse of 405-nm laser, and imaging was performed with a 1.5-s frame rate. To generate a fluorescent decay trace, the ratio of photoconverted (red) signal in the brush border and the total amount of red signal in the cell were determined for each time point. Moving regions of interest were drawn to correct for cell movements during imaging. Ratios were normalized and multiple traces were averaged to generate a mean fluorescence decay trace. Single exponential curve fitting was performed on the mean decay traces using MATLAB software with the general formula: $f(x) = a \cdot e^{(-b \cdot x)} + c$. A mean half-life was determined using the fitted curve. For statistical analyses, half-lives of the individual decay traces were determined and compared using an independent samples *t* test in SPSS with a p-value <0.05 as a cutoff for significance.

Online supplemental material

Fig. S1 complements Fig. 1 in demonstrating that ATP8B1 affects lumen formation but does not affect segregation of the polarization markers pERM, CD71, and ZO-1. Fig. S1 (D and E) demonstrates altered bile canalicular lumen formation in *ATP8B1*$^{G308V/G308V}$ mice. Fig. S2 shows the distribution of polarity markers in normal and ATP8B1-depleted W4 cells. Fig. S3 complements Fig. 5 in demonstrating that mobility of the Rap2 HVR is not affected by ATP8B1 depletion. Fig. S3 C contains the quantification of the residential half-lives from Fig. 5 E. Online supplemental material is available at http://www.jcb.org/cgi/content/full/jcb.201505118/DC1.

Acknowledgements

This paper is dedicated to the memory of Alan Hall and Chris Marshall, pioneers and leaders of the small GTPase field.

We thank Bas Ponsioen for assistance in microscopy and data analysis, Hugo Snippert for help in organoid culture establishment, Cilia de Heus for technical assistance with electron microscopy, Kees Hoeben for quantification of canalicular lumen area, Johan Offerhaus for histopathologic evaluation of patient biopsy materials, and J. van Velzen and P. van der Burght for technical assistance with FACS sorting. We thank Martijn Gloerich for comments on the manuscript and all members of the Bos laboratory for continuous support and discussion.

The authors declare no competing financial interests.

Submitted: 28 May 2015
Accepted: 5 August 2015

References

Baas, A.F., J. Kuipers, N.N. van der Wel, E. Batlle, H.K. Koerten, P.J. Peters, and H.C. Clevers. 2004. Complete polarization of single intestinal epithelial cells upon activation of LKB1 by STRAD. *Cell.* 116:457–466. http://dx.doi.org/10.1016/S0092-8674(04)00114-X

Bryant, D.M., and K.E. Mostov. 2008. From cells to organs: building polarized tissue. *Nat. Rev. Mol. Cell Biol.* 9:887–901. http://dx.doi.org/10.1038/nrm2523

Bryant, D.M., A. Datta, A.E. Rodríguez-Fraticelli, J. Peränen, F. Martín-Belmonte, and K.E. Mostov. 2010. A molecular network for de novo generation of the apical surface and lumen. *Nat. Cell Biol.* 12:1035–1045. http://dx.doi.org/10.1038/ncb2106

Bull, L.N., V.E. Carlton, N.L. Stricker, S. Baharloo, J.A. DeYoung, N.B. Freimer, M.S. Magid, E. Kahn, J. Markowitz, F.J. DiCarlo, et al. 1997. Genetic and morphological findings in progressive familial intrahepatic cholestasis (Byler disease [PFIC-1] and Byler syndrome): evidence for heterogeneity. *Hepatology.* 26:155–164. http://dx.doi.org/10.1002/hep.510260121

Bull, L.N., M.J. van Eijk, L. Pawlikowska, J.A. DeYoung, J.A. Juijn, M. Liao, L.W. Klomp, N. Lomri, R. Berger, B.F. Scharschmidt, et al. 1998. A gene encoding a P-type ATPase mutated in two forms of hereditary cholestasis. *Nat. Genet.* 18:219–224. http://dx.doi.org/10.1038/ng0398-219

Cai, S.Y., S. Gautam, T. Nguyen, C.J. Soroka, C. Rahner, and J.L. Boyer. 2009. ATP8B1 deficiency disrupts the bile canalicular membrane bilayer structure in hepatocytes, but FXR expression and activity are maintained. *Gastroenterology.* 136:1060–1069: 1069.e4. http://dx.doi.org/10.1053/j.gastro.2008.10.025

Caviston, J.P., S.E. Tcheperegine, and E. Bi. 2002. Singularity in budding: a role for the evolutionarily conserved small GTPase Cdc42p. *Proc. Natl. Acad. Sci. USA.* 99:12185–12190. http://dx.doi.org/10.1073/pnas.182370299

Das, A., B.D. Slaughter, J.R. Unruh, W.D. Bradford, R. Alexander, B. Rubinstein, and R. Li. 2012. Flippase-mediated phospholipid asymmetry promotes fast Cdc42 recycling in dynamic maintenance of cell polarity. *Nat. Cell Biol.* 14:304–310. http://dx.doi.org/10.1038/ncb2444

Dhekne, H.S., N.H. Hsiao, P. Roelofs, M. Kumari, C.L. Slim, E.H. Rings, and S.C. van Ijzendoorn. 2014. Myosin Vb and Rab11a regulate phosphorylation of ezrin in enterocytes. *J. Cell Sci.* 127:1007–1017. http://dx.doi.org/10.1242/jcs.137273

Finkielstein, C.V., M. Overduin, and D.G. Capelluto. 2006. Cell migration and signaling specificity is determined by the phosphatidylserine recognition motif of Rac1. *J. Biol. Chem.* 281:27317–27326. http://dx.doi.org/10.1074/jbc.M605560200

Forget, M.A., R.R. Desrosiers, D. Gingras, and R. Béliveau. 2002. Phosphorylation states of Cdc42 and RhoA regulate their interactions with Rho GDP dissociation inhibitor and their extraction from biological membranes. *Biochem. J.* 361:243–254. http://dx.doi.org/10.1042/bj3610243

Gervais, L., S. Claret, J. Januschke, S. Roth, and A. Guichet. 2008. PIP5K-dependent production of PIP2 sustains microtubule organization to establish polarized transport in the *Drosophila* oocyte. *Development.* 135:3829–3838. http://dx.doi.org/10.1242/dev.029009

Goryachev, A.B., and A.V. Pokhilko. 2008. Dynamics of Cdc42 network embodies a Turing-type mechanism of yeast cell polarity. *FEBS Lett.* 582:1437–1443. http://dx.doi.org/10.1016/j.febslet.2008.03.029

Howell, A.S., N.S. Savage, S.A. Johnson, I. Bose, A.W. Wagner, T.R. Zyla, H.F. Nijhout, M.C. Reed, A.B. Goryachev, and D.J. Lew. 2009. Singularity in polarization: rewiring yeast cells to make two buds. *Cell.* 139:731–743. http://dx.doi.org/10.1016/j.cell.2009.10.024

Klünder, B., T. Freisinger, R. Wedlich-Söldner, and E. Frey. 2013. GDI-mediated cell polarization in yeast provides precise spatial and temporal control of Cdc42 signaling. *PLOS Comput. Biol.* 9:e1003396. http://dx.doi.org/10.1371/journal.pcbi.1003396

Marco, E., R. Wedlich-Soldner, R. Li, S.J. Altschuler, and L.F. Wu. 2007. Endocytosis optimizes the dynamic localization of membrane proteins that regulate cortical polarity. *Cell.* 129:411–422. http://dx.doi.org/10.1016/j.cell.2007.02.043

Martin-Belmonte, F., A. Gassama, A. Datta, W. Yu, U. Rescher, V. Gerke, and K. Mostov. 2007. PTEN-mediated apical segregation of phosphoinositides controls epithelial morphogenesis through Cdc42. *Cell.* 128:383–397. http://dx.doi.org/10.1016/j.cell.2006.11.051

Paulusma, C.C., A. Groen, C. Kunne, K.S. Ho-Mok, A.L. Spijkerboer, D. Rudi de Waart, F.J. Hoek, H. Vreeling, K.A. Hoeben, J. van Marle, et al. 2006. Atp8b1 deficiency in mice reduces resistance of the canalicular membrane to hydrophobic bile salts and impairs bile salt transport. *Hepatology.* 44:195–204. http://dx.doi.org/10.1002/hep.21212

Paulusma, C.C., D.E. Folmer, K.S. Ho-Mok, D.R. de Waart, P.M. Hilarius, A.J. Verhoeven, and R.P. Oude Elferink. 2008. ATP8B1 requires an accessory protein for endoplasmic reticulum exit and plasma membrane lipid flippase activity. *Hepatology.* 47:268–278. http://dx.doi.org/10.1002/hep.21950

Pawlikowska, L., A. Groen, E.F. Eppens, C. Kunne, R. Ottenhoff, N. Looije, A.S. Knisely, N.P. Killeen, L.N. Bull, R.P. Elferink, and N.B. Freimer. 2004. A mouse genetic model for familial cholestasis caused by ATP8B1 mutations reveals perturbed bile salt homeostasis but no impairment in bile secretion. *Hum. Mol. Genet.* 13:881–892. http://dx.doi.org/10.1093/hmg/ddh100

Rodriguez-Boulan, E., and I.G. Macara. 2014. Organization and execution of the epithelial polarity programme. *Nat. Rev. Mol. Cell Biol.* 15:225–242. http://dx.doi.org/10.1038/nrm3775

Saito, K., K. Fujimura-Kamada, H. Hanamatsu, U. Kato, M. Umeda, K.G. Kozminski, and K. Tanaka. 2007. Transbilayer phospholipid flipping regulates Cdc42p signaling during polarized cell growth via Rga GTPase-activating proteins. *Dev. Cell.* 13:743–751. http://dx.doi.org/10.1016/j.devcel.2007.09.014

Sato, T., R.G. Vries, H.J. Snippert, M. van de Wetering, N. Barker, D.E. Stange, J.H. van Es, A. Abo, P. Kujala, P.J. Peters, and H. Clevers. 2009. Single Lgr5 stem cells build crypt-villus structures in vitro without a mesenchymal niche. *Nature.* 459:262–265. http://dx.doi.org/10.1038/nature07935

Slaughter, B.D., S.E. Smith, and R. Li. 2009. Symmetry breaking in the life cycle of the budding yeast. *Cold Spring Harb. Perspect. Biol.* 1:a003384. http://dx.doi.org/10.1101/cshperspect.a003384

Slaughter, B.D., J.R. Unruh, A. Das, S.E. Smith, B. Rubinstein, and R. Li. 2013. Non-uniform membrane diffusion enables steady-state cell polarization via vesicular trafficking. *Nat. Commun.* 4:1380. http://dx.doi.org/10.1038/ncomms2370

Ujhazy, P., D. Ortiz, S. Misra, S. Li, J. Moseley, H. Jones, and I.M. Arias. 2001. Familial intrahepatic cholestasis 1: studies of localization and function. *Hepatology.* 34:768–775. http://dx.doi.org/10.1053/jhep.2001.27663

van der Woerd, W.L., S.W. van Mil, J.M. Stapelbroek, L.W. Klomp, S.F. van de Graaf, and R.H. Houwen. 2010. Familial cholestasis: progressive familial intrahepatic cholestasis, benign recurrent intrahepatic cholestasis and intrahepatic cholestasis of pregnancy. *Best Pract. Res. Clin. Gastroenterol.* 24:541–553. http://dx.doi.org/10.1016/j.bpg.2010.07.010

van Mil, S.W., M.M. van Oort, I.E. van den Berg, R. Berger, R.H. Houwen, and L.W. Klomp. 2004. Fic1 is expressed at apical membranes of different epithelial cells in the digestive tract and is induced in the small intestine during postnatal development of mice. *Pediatr. Res.* 56:981–987. http://dx.doi.org/10.1203/01.PDR.0000145564.06791.D1

Wedlich-Soldner, R., S. Altschuler, L. Wu, and R. Li. 2003. Spontaneous cell polarization through actomyosin-based delivery of the Cdc42 GTPase. *Science.* 299:1231–1235. http://dx.doi.org/10.1126/science.1080944